Spatially–resolved luminescence properties of etched quantum well microstructures

J P Landesman, E Diak, R R Lapierre, C Levallois, S Ghanad-Tavakoli

Journal of Applied Physics

Spatially–resolved luminescence properties of etched quantum well microstructures

J. P. Landesman,[1] E. Diak,[2] R. R. LaPierre,[2] C. Levallois,[1] and S. Ghanad–Tavakoli[2]
[1)]*Univ Rennes, INSA Rennes, CNRS, Institut FOTON–UMR 6082, F-35000 Rennes, France.*
[2)]*Department of Engineering Physics, McMaster University, Hamilton, ON L8S 4L7, Canada.*

(*Electronic mail: jean-pierre.landesman@univ-rennes.fr.)

(Dated: 28 August 2024)

Ridge microstructures were prepared by etching through samples consisting of a series of stacked $InAs_xP_{1-x}$ quantum wells (QWs) with step graded composition grown on InP by molecular beam epitaxy. Different etching techniques were used: wet etching with HCl/H_2O and reactive ion etching (RIE) with CH_4/H_2. These microstructures were characterized by low temperature micro–photoluminescence. The photoluminescence (PL) emission associated with each QW was clearly identified. The PL was measured in detail across etched ridge stripes of various widths. Variations of the integrated PL intensities across the etched stripes were observed. The PL intensities for all QWs increase gradually from the edge to the center of the ridge microstructures. The PL intensity measured at the ridge center is systematically reduced for ridges which are 10 or 20 μm wide as compared to ridges which are 30 μm wide or larger. On the other hand, the spectral peak position of the PL lines remained constant with high accuracy (0.2 to 0.4 meV) across the microstructures. These observations are discussed in terms of the different possible mechanisms which determine the PL intensity variations, namely non–radiative recombination at the etched walls and effects of stray electric fields which result from the etching process. Based on this discussion, we compare quantitatively the different etching processes which we have used. Altogether, this study illustrates the contribution that specially designed test structures, coupled with advanced spectroscopic characterization, can provide to the development of semiconductor photonic devices (e.g. lasers or waveguides) involving etching processes.

I. INTRODUCTION

The fabrication schemes for photonic devices based on III–V semiconductor materials and heterostructures usually involve critical steps such as etching for the definition of waveguides. Etching determines the critical dimensions and shape of waveguides. It can also generate degradation of the materials' electronic and optical properties. Such degradation can be identified and characterized through carrier lifetime measurements[1], photoluminescence (PL) measurements, especially quantum well (QW) PL intensity degradation[2], and modification of devices' parameters[3–6]. Two classes of etching process are mainly used for III–V semiconductors when considering photonic device fabrication : wet etching and reactive ion etching (RIE), also designated as plasma etching. These differ in terms of the isotropic / anisotropic etching mechanism. Wet etching generally results either in an isotropic shape of the etched surface or in an etching sensitive to the crystallographic orientation, where crystallographic planes are revealed[7,8]. RIE allows for an improved control of the etching process and in particular a better transfer of micro or nanometric patterns in the material, thanks to the anisotropic nature of the process[9]. The etching processes also differ in terms of the fundamental mechanisms which take place at the semiconductor surface during the etching. For wet etching, liquid phase chemical reactions involving the semiconductor and the etchant solution govern the evolution of the microstructure to be defined. For RIE, etching proceeds through a synergistic combination of chemical reactions and physical sputtering due to energetic ions generated in the plasma[10]. In this article, we address the question of how different etching processes affect the fabricated microstructures, such as waveguides, especially for the optoelectronic properties. For this purpose, we have fabricated ridge structures by etching through heterostructure materials containing QWs with different spectral characteristics and analyzed their PL using a spatially resolved, low temperature set–up which allows us to probe the etched structures at a local scale.

II. SAMPLE PREPARATION

The samples were grown by gas source molecular beam epitaxy (MBE) on InP(100) n–doped (10^{18} cm^{-3}) substrates. A series of 8 $InAs_xP_{1-x}$ QWs were buried at different depths below the surface. These QWs had a constant thickness (typically between 7 and 8 *nm*) and a graded As/P composition. The thickness for the InP barriers was 100 *nm*. The growth temperature was 470 °C. A solid source was used for In, whereas gas crackers (with PH_3 and AsH_3) produced P_2 and As_2 fluxes. The positions of the QWs with different As compositions (i.e. different energy gaps) were carefully chosen to avoid absorption of the PL signals as they travel through the upper–lying QWs[11,12]. The QWs and InP buffer and barriers were grown undoped.

These samples were covered by a 500 *nm* thick SiN_y hard mask layer deposited at 250 °C by plasma enhanced chemical vapor deposition. Stripes of various widths (1 to 50 μm) and a length of several *mm* were subsequently defined by optical lithography in this hard mask layer. The stripes were then transferred into the semiconductor material using two different etching processes to compare wet and dry etching. Wet etching was ensured by a minute immersion in a concentrated hydrochloric acid solution (30 %) followed by a minute rinsing with an abundant flow of deionized water. For such a so-

lution, etching kinetics of several $\mu m/min$ are generally observed in InP[13]. Here the etching depth was estimated around 4 μm. For the dry etching process, a capacitively coupled RIE reactor with CH_4/H_2/Ar gas mixture was used. In this reactor, the sample was attached to a water-cooled sample holder and was exposed to the plasma for 1 hour to achieve an etching depth around 1 μm. The plasma power applied during the etching process is moderate and limited to 40 W over the 2 " wafer with a flow ratio between the CH_4/H_2/Ar gases as follows: 3/6/1. The residual pressure within the etching chamber is lower than 10^{-5} *mbar* before etching process and increases to $5.6 \cdot 10^{-2}$ *mbar* during gas injection.

After the stripes fabrication, the remaining SiN_y hard mask was removed in a buffered HF solution. Fig. 1 illustrates the schematic sample structure after etching. As indicated, the QWs are numbered from the surface to the bulk of the sample. QW #1 has the lowest *As* composition (highest energy bandgap) while QW #8 has the highest *As* composition and lowest energy bandgap.

Scanning electron micrographs of etched stripes are shown in fig. 2. The RIE process produces nearly vertical sidewalls with a small sub–μm step near the top surface. This step can be related to the vertical etch rate which is lower for the $InAs_xP_{1-x}$ QWs material than for InP. Because of this difference, the QWs material slightly etches laterally during the vertical etch. The wet etching reveals sidewalls which are crystallographic planes with a (111)–type of orientation for the case where the elongated stripe orientation is perpendicular to the small flat, i.e. along the $< 0 \quad \bar{1} \quad 1 >$ direction. For the perpendicular orientation $< 0 \quad \bar{1} \quad \bar{1} >$, wet etching produces sidewalls which have a (110)– type of orientation at the top and a (111)–type of orientation at the bottom. This probably results from a competition between the etch rate for both crystal plane orientations. Only stripes parallel to the $< 0 \quad \bar{1} \quad 1 >$ direction were used for the dry etching process. It can be noticed also that wet etched stripes have a vertical dimension of more than 4 μm while the RIE stripes have been etched slightly over 1 μm (i.e. deep enough to expose all the QWs to the sidewalls), demonstrating a much easier control over the etch rate with the RIE process than with the wet etching process, as already mentioned.

III. LOW TEMPERATURE MICRO-PHOTOLUMINESCENCE MEASUREMENTS

Low–temperature micro–PL (μPL) experiments were conducted at 10 K in a specially designed optical cryostat[14]. The spectrometer for this set-up is an asymmetric Czerny-Turner type (Model iHR550) made by Horiba Jobin Yvon. The focal length is 0.55 m. Detection is made using an InGaAs photodiode. A 600 gr/mm grating was used, providing a spectral resolution slightly over 0.025 nm. The excitation wavelength was 1064 nm (from a CW Nd:YAG laser) with a diffraction–limited spot size below 1 μm. This wavelength corresponds to a photon energy smaller than the InP band gap, but larger than the band gap of the $InAs_xP_{1-x}$ QWs. Thus, excitation of electron–hole pairs within the InP barriers does not occur. The excitation power density was approximately 10^6 W/cm^2 (however, only a small part of this power density contributes to excitation of electron–hole pairs within the QWs). Fig. 3-a shows a typical spectrum measured at 10 K from a sample immediately after MBE growth.

The PL signal from the 8 QWs can be clearly identified through very sharp lines, which appear unique for each QW. We propose that this is due to the low excitation power density and to the separation between light hole (LH) and heavy hole (HH) energy levels in the $InAs_xP_{1-x}$ QWs induced by the compressive stress, which was estimated to be of the order of 0.1 eV[15,16]. This energy separation allows transitions from the electron to the HH level, the LH level lying too high in energy for the corresponding transitions to be excited at low pumping power density. Fig. 3-b shows the transition energies deduced from the experimental spectrum. We have calculated the QW transition energies within an envelope function / effective mass approximation, using the Nextnano software[17]. The strain in the $InAs_xP_{1-x}$ QWs was taken into account. Materials' parameters (in particular dependence of the effective masses for the first electron and HH levels on the As composition and strain) were taken from the Nextnano database. An exciton binding energy of 14 meV was chosen, as suggested by the calculation by[18]. We have run these calculations for QW thicknesses equal to 7.5 nm, and the nominal As compositions chosen during growth of the sample. The results from these calculations are displayed in fig. 3-b by the red symbols. For the highest As compositions, the experimental data match very well with the theoretical data. As the As composition decreases, an increasing difference is observed, which is probably due partly to strain relaxation and also to some excess As incorporation in the QWs and / or in the InP barriers as sample growth proceeds.

An analytical model was used to extract relevant spectral information. This model provides best–fits to the experimental data with a series of Gaussian line–shapes, as described by Eq. 1.

$$I_{PL}(\lambda) = \sum_{i=1}^{8} A_i \cdot exp\left(-\frac{(\lambda-\lambda_i)^2}{2 \cdot FWHM_i^2}\right) \qquad (1)$$

where, for each of the eight PL lines, A_i denotes the amplitude, λ_i the central wavelength and $FWHM_i$ the full width at half maximum. From these parameters, the integrated intensity for each PL line can be determined. Fig. 3-a also illustrates this fitting procedure.

As indicated in Fig.1, μPL measurements were performed by scanning the laser beam across the etched ridges, in the perpendicular direction. The step–size during these linescans was $5 \pm 1 \mu m$ (the $\pm 1 \mu m$ accuracy is mainly due to scale reading). However the spot size was diffraction-limited to approximately 1 μm . In order to assess the actual spatial resolution for these μPL measurements, a linescan was performed across the cleaved edge of the sample immediately after MBE growth. The integrated intensity for the PL line associated to QW #4, as a function of the laser spot position, as illustrated in fig. 4. A best fit of this intensity variation was performed

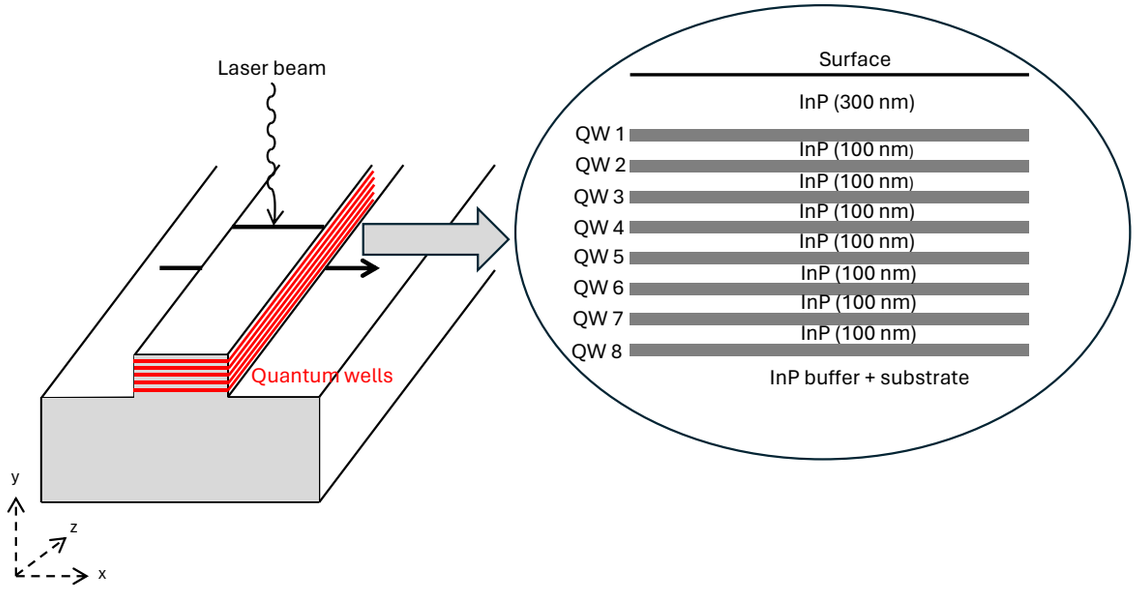

FIG. 1. Epitaxial sample structure. Each $InAs_xP_{1-x}$ QW has the same thickness (7.5 nm). The As/(P+As) composition is step graded, from 0.49 for QW8 to 0.35 for QW1.

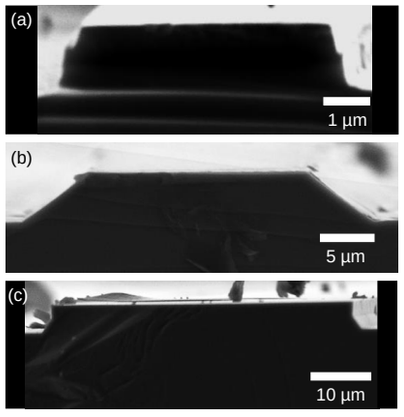

FIG. 2. Secondary electron micrographs of etched stripes, cross section. (a) Dry etched, $< 0 \quad \bar{1} \quad 1 >$ orientation, width 5 μm. (b) Wet etched, $< 0 \quad \bar{1} \quad 1 >$ orientation, width 20 μm. (c) Wet etched, $< 0 \quad \bar{1} \quad \bar{1} >$ orientation, width 50 μm.

using the equation

$$I(X) = \left(\frac{I_{inf}}{2}\right) erfc\left(\frac{X - X_0}{\sigma}\right) \tag{2}$$

where

- $erfc$ is the complementary error function
- X is the position (in μm) for the laser spot
- X_0 (in μm) is the position for the cleaved edge
- I_{inf} is the intensity very far from the edge
- σ (in μm) is a parameter describing the spatial resolution

The procedure was repeated for several measurements, and produced highly variable values for the σ parameter (typically between less than 1 μm and almost 5 μm for different series of similar profiles). The reason for this variability was investigated using simulated intensity profiles obtained by convolution of a gaussian illumination spot (with width parameter 1 μm) with a Heaviside profile representing the cleaved edge. The best fit procedure using eq. 2 was applied to these simulated intensity profiles. It was thus realized that the limited accuracy on the step size, $\pm 1 \mu m$, which results in some inaccuracy on the position of the laser spot during profile recordings, is the main cause for the variability on the σ parameter

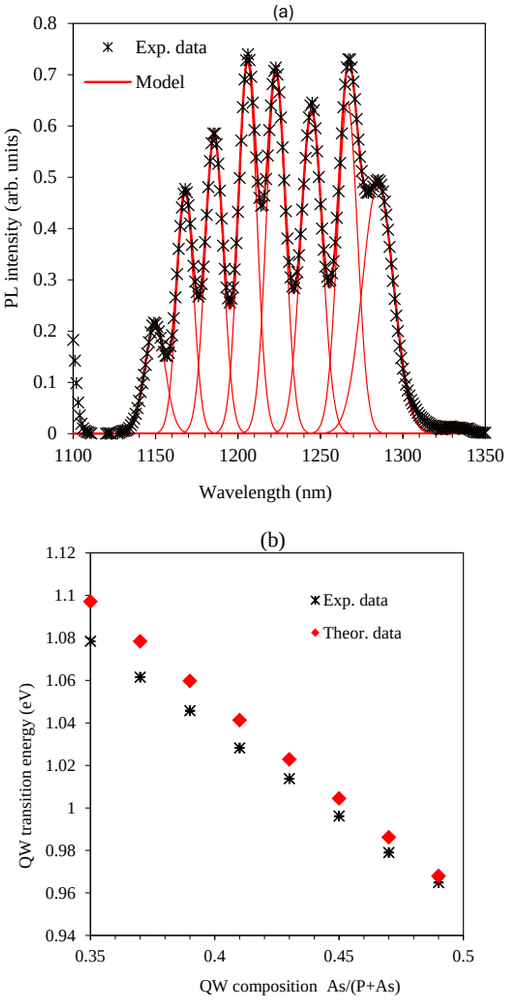

FIG. 3. (a) Low temperature (10 K) PL spectrum measured after epitaxial growth. Black symbols ($*$): experimental data; red line : best–fit with the model described in the text. (b) QW transition energies versus As composition. Black symbols ($*$): experimental data (PL peak energies); Red symbols ($\blacklozenge$): calculated peak energies.

determination. Based on these observations, we think that any value smaller than 5 μm is affected by an artefact, only variations of the PL peak intensities occurring on a length scale larger than 5 μm should be discussed..

Figure 5 shows the PL intensity profiles measured for 10, 20, 30 and 50 μm stripes etched with the RIE process. The experimental values are the integrated intensities for the different QWs, as obtained from the best fit procedure to the μPL spectra described previously. In order to highlight and quantify the differences these experimental intensity profiles were described using a best fit procedure adapted from the previous analytical function. As the PL excitation pump beam passes through the rising and falling profile of the stripes, a sum of

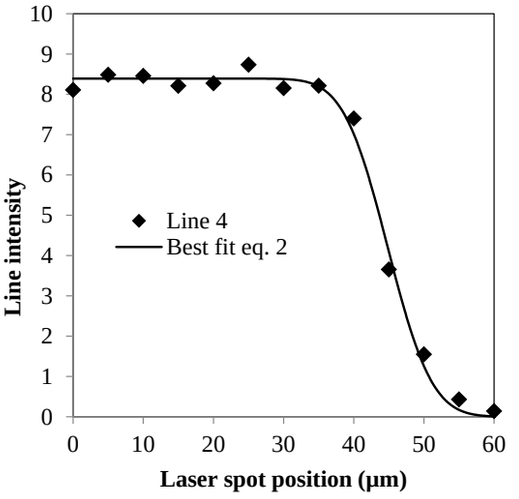

FIG. 4. Intensity profile for QW #4 as a function of the laser spot position across a cleaved edge on the reference MBE sample. The best fit curve, obtained using eq. 2, is also shown.

$erfc$ and erf functions was therefore used:

$$I(X) = \left(\frac{I_{inf}}{2}\right)\left[erfc\left(\frac{X-X_r}{\sigma}\right) + erf\left(\frac{X-X_l}{\sigma}\right)\right] \quad (3)$$

where X_l and X_r (in μm) are the positions for the left and right edges of the stripe.

This best fit procedure involves 4 adjustable parameters. The corresponding functions are indicated in fig. 5 in solid lines.

One can observe in fig. 5 several significant trends :

- The integrated PL line intensity increases gradually at both edges
- For 30 and 50 μm stripes the intensity reaches the same maximum
- For 10 and 20 μm stripes the intensity at the stripe center is significantly smaller than for 30 and 50 μm stripes; note that this is not a matter of experimental spatial resolution (even though the step size is 5 μm) because the spot size is diffraction limited. We have checked this very carefully by reproducing the measurements several times.
- The intensity reduction for narrower stripes (for example 10 μm compared to 30 and 50 μm) appears more important for lines corresponding to QWs close to the sample surface than for deeper QWs.

The intensity profiles measured on the wet etched stripes with $< 0 \quad \bar{1} \quad 1 >$ orientation are displayed in fig. 6. The same general observations as made for the dry etched stripes can be done, but comparison between both types of stripes shows a lower PL intensities for wet etched stripes. Fig. 7 displays the results for wet etched stripes with $< 0 \quad \bar{1} \quad \bar{1} >$ orientation.

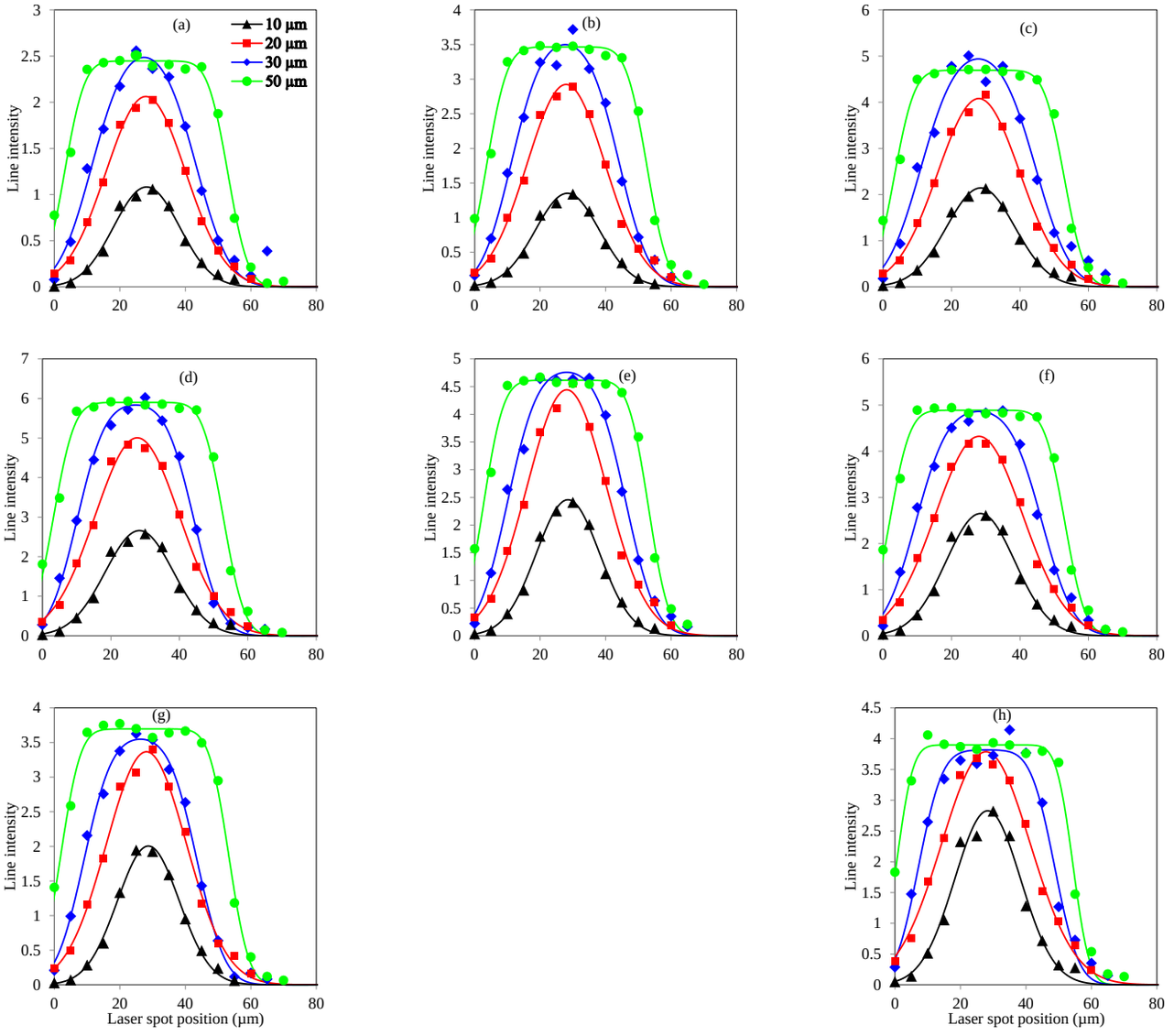

FIG. 5. Intensity profiles deduced from the best–fit procedure to the experimental spectra for the different QWs, for stripes of width 10, 20, 30 and 50 μm obtained using the RIE process ($< 0 \quad \bar{1} \quad 1 >$ orientation). The experimental intensity values are indicated by symbols (green ● : 50 μm; blue ♦ : 30 μm; red ■ : 20 μm; black ▲ : 10 μm). The solid lines are the best fit to the experimental intensities using the $erf/erfc$ model described in the text by eq. 3. (a) QW #1; (b) QW #2; (c) QW #3; (d) QW #4; (e) QW #5; (f) QW #6; (g) QW #7; (h) QW #8.

Note that only 10, 20 and 30 μm stripes were measured on this sample. We again observe that the PL intensities for this sample are lower than for the dry etched one. The intensity reduction associated to reducing stripe width ($30 > 20 > 10$ μm) is much less pronounced for this sample than for the other ones.

The spectral positions for the PL lines (deduced from the best fit procedure for the experimental spectra measured at each point across the ridges) were also analyzed. The results for a 50 μm RIE stripe are shown in fig. 8. For clarity we have superimposed in fig. 8 the intensity profile and the spectral position. The spectral position varies by less than 0.25 *nm* within the stripe, even if some data points indicate slightly stronger shifts, they correspond to locations outside the stripe and the spectrum intensity is too low for the values to be considered meaningful. Similar observations were made for both types of stripes, and for all different widths. Based on previous work[11,12] we consider that the spectral shifts are not significant.

IV. DISCUSSION

The first noticeable observation in our measurements is the gradual increase in the PL intensity from both etched walls in the stripes. Depending on the samples, this increase occurs

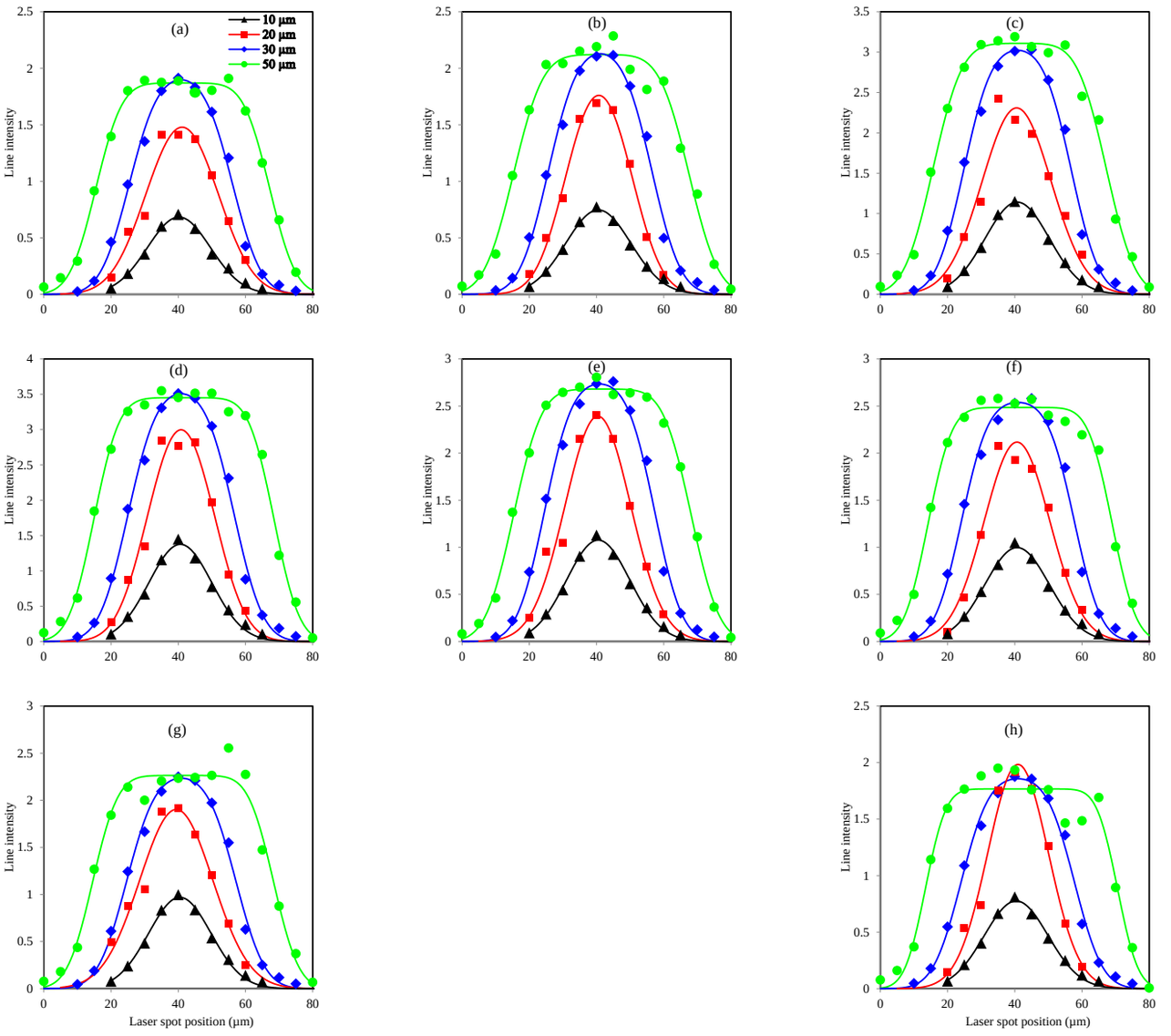

FIG. 6. Intensity profiles deduced from the best–fit procedure to the experimental spectra for the different QWs, for stripes of width 10, 20, 30 and 50 μm obtained using the wet etched process ($< 0 \quad \bar{1} \quad 1 >$ orientation). The experimental intensity values are indicated by symbols (green ● : 50 μm; blue ♦ : 30 μm; red ■ : 20 μm; black ▲ : 10 μm). The solid lines are the best fit to the experimental intensities using the $erf/erfc$ model described in the text by eq. 3. (a) QW #1; (b) QW #2; (c) QW #3; (d) QW #4; (e) QW #5; (f) QW #6; (g) QW #7; (h) QW #8.

over distances of the order of up to 10 μm. Related to this gradual increase – and clearly a consequence of it – we observed that for stripes whose width is 10 or 20 μm the PL intensity does not reach its maximum at the stripe center, while for stripes whose width is 30 or 50 μm it does reach its maximum in the center region. This point is of importance for photonic devices with waveguides or stripes similar to the ones we have investigated. Since their luminescence efficiency might be reduced due to the geometrical features and the etching process, the optoelectronic performance may also be affected.

A mechanism suggested for the decrease of the PL intensity near a free surface is non-radiative recombination, characterized by a surface recombination velocity[19,20]. This mechanism can impact the PL intensity measured at distances smaller than the charge carrier diffusion length from the free surface. The charge carrier diffusion length is a very important parameter in the analysis of PL intensity profiles. It is determined by different fundamental parameters in semiconductor materials: the recombination rates for the different recombination processes (non-radiative recombination, spontaneous emission, Auger recombination), and the diffusion coefficient. Some of these parameters vary with temperature and the charge carrier concentration. Becht et al.[21] for example describe the usual model to compute the diffusion length in QW structures. Published diffusion lengths in QW structures vary over a wide range depending on the materials, on

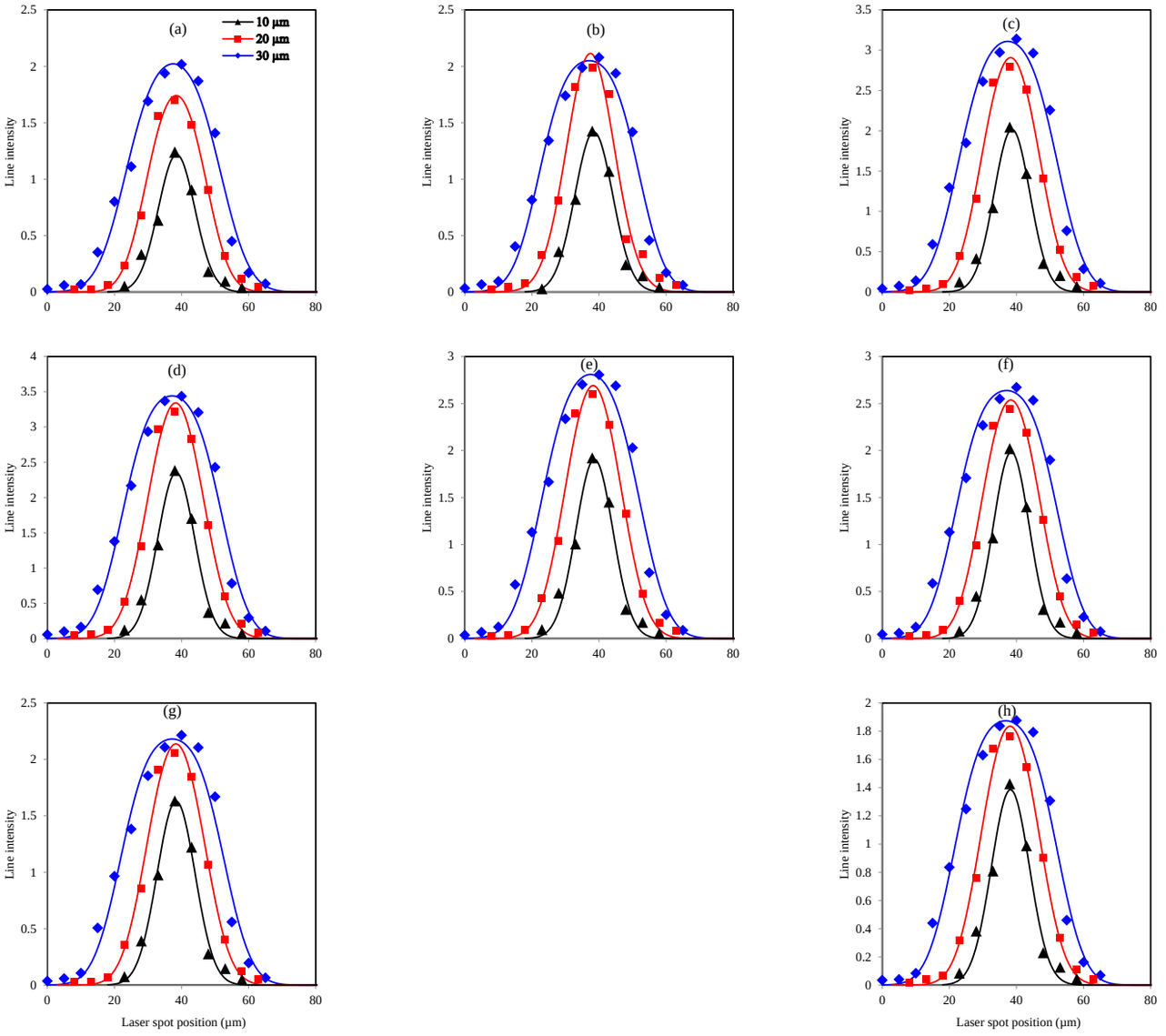

FIG. 7. Intensity profiles deduced from the best–fit procedure to the experimental spectra for the different QWs, for stripes of width 10, 20 and 30 μm obtained using the wet etched process ($< 0 \quad \bar{1} \quad \bar{1} >$ orientation). The experimental intensity values are indicated by symbols (blue ♦ : 30 μm; red ■ : 20 μm; black ▲ : 10 μm). The solid lines are the best fit to the experimental intensities using the $erf/erfc$ model described in the text by eq. 3. (a) QW #1; (b) QW #2; (c) QW #3; (d) QW #4; (e) QW #5; (f) QW #6; (g) QW #7; (h) QW #8.

the carrier injection mechanisms, temperature, etc. Values as large as a few μm have been published recently for nitride-based QWs[21], but for the case of arsenide- and phosphide-based QWs the ambipolar diffusion lengths were observed of the order of 1 μm at most, especially for QW samples similar to the ones grown for the present study[22,23]. Based on this consideration, we assert that the non-radiative surface recombination velocity at the etched sidewalls alone cannot explain the quenching of the PL intensity which we observe, although it can contribute. An additional mechanism, with some kind of "long range" effect, must be proposed. We can think of two possible physical issues which may affect the radiative recombination over a "long" distance in our stripe samples, i.e. a distance comparable to their width. The first issue is strain relaxation within the QWs: incorporation of *As* in the QWs induces biaxial compressive strain, which potentially may be relaxed in the vicinity of the etched sidewalls. Strain relaxation is known to occur over several μm and also to affect the strength of the optical transitions in the QWs. Strain relaxation should affect the spectral shape of the PL lines, in particular their position and FWHM. Fig. 8 shows the variation in the line position measured within one of the stripes: the amount is limited to a small fraction of a *nm*, while typical values expected should reach several *nm*[24]. Our measurements also showed that the FWHM of the different lines does not change significantly over the linescans. It is actually quite

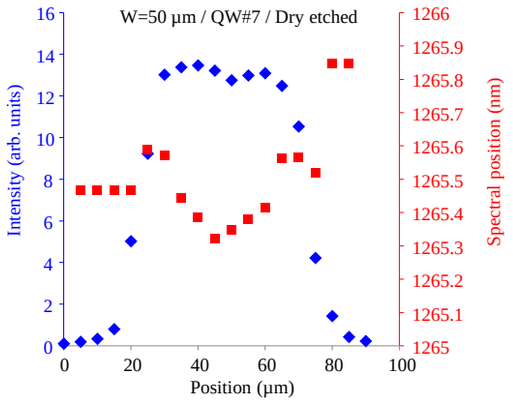

FIG. 8. Intensity profile (blue ♦) and spectral position (red ■) for QW #7 for a 50 μm RIE stripe.

easy to explain that the compressive strain in the QWs should not relax significantly upon etching the ridge sidewalls. The InP substrate itself cannot change its lattice parameter, therefore etching should not lead to significant strain relaxation within the QWs at stripe edges.

The second possible physical issue for the "long range" effect is an electric field generated by charges accumulated at etched sidewalls. We assume that the etching process could lead to accumulation of charged ions at the sidewalls, especially when halogens are involved. This was actually demonstrated for the case of F in Si etching[25]. These implanted ions could generate an electric field with an extension covering a part of the stripe width. Electric fields in the range of a few kV/cm, parallel to the sample surface, can induce significant exciton quenching, and thus PL intensity decrease, as was shown by[26]. We propose that this interaction of an electric field due to implantation of charged ions resulting from the etching process with the photogenerated electron–hole pairs could explain our observations. Actually, the complete quantitative description of our results requires a model which couples the non-radiative recombination mechanisms at the etched sidewalls with this electric field effect. This will be the next step of our study.

To compare quantitatively our different etching conditions, we have plotted in fig. 9 normalized PL intensities for the series of 8 QWs, for the different stripe widths and for the different etching conditions. The intensity values used for fig. 9 are those for the maximum on the profiles displayed in figs. 5 to 7. For the normalization procedure we used the intensities measured on the reference, un-etched sample immediately after epitaxial growth. The first observation is that the PL intensities are higher for the RIE samples than for the wet etched samples. The reason for this difference is under current investigation. Next, we can see that for the RIE sample the relative intensities for the series of QWs appear quite similar to that for the reference sample: the values for the normalized intensities fluctuate about an average value, except maybe for QW #8 which deviates significantly from the average. QW #8 is grown first, and therefore located closest to the substrate / epitaxial buffer interface. The average value in fig. 9 a-c indicates that the RIE process slightly degrades the PL intensity initially measured for the reference sample. The magnitude of this degradation is larger for a stripe width of 10 and 20 μm than for 30 μm. This trend is already obvious from fig. 5. Based on the observations we can assess that the electric field in our assumption has roughly the same value for the different QWs (except for QW #8) in the RIE stripes.

For the wet etched stripes with $< 0 \quad \bar{1} \quad 1 >$ orientation, fig. 9 shows that the normalized intensity decreases gradually from QW #1 to QW #8, even though a slight increase is seen between QW #7 and QW #8. This adds to the observations made for fig. 6, namely that for this sample the 10 and 20 μm stripes display a strongly reduced overall intensity as compared to 30 and 50 μm. For the wet etched stripes with $< 0 \quad \bar{1} \quad \bar{1} >$ orientation, a gradual decrease from QW #1 to QW #8 is also observed but, as already deduced from fig. 7, the PL intensities do not decrease as much as the stripe width reduces as for the other samples. In the framework of our assumption for the presence of an electric field in these etched samples, the observations for the wet etched stripes leads us to conclude that the magnitude of the electric field increases from QW #1 to QW #8 for these samples. In the absence of a characterization of the chemical nature of the surfaces at the etched sidewalls we cannot get more information on the possible causes for the differences observed during our investigations on different etching processes (and different orientations for the stripes). However, we have clearly demonstrated trends on the QW PL intensities. The trends are the signature of a degradation mechanism which may strongly influence the performance of photonic devices made using materials similar to the ones used in this study (such as laser diodes, passive waveguides, ...).

V. CONCLUSION

Our μPL experiments on QW etched microstructures have shown that the PL intensity is strongly affected by the proximity of the etched sidewalls. The PL intensity gradually decreases when approaching these sidewalls, over a distance of several μm. As a consequence of this trend, stripes having a width of 10 or 20 μm do not allow the PL signal from the QWs to reach the maximum intensity as in larger stripes. This has important potential consequences for devices such as waveguides or laser diodes, where the opto-electronic properties might be affected by the etching process. Our experiments have also shown that the magnitude of this effect depends on the type of etching process (RIE or wet etching), and the stripe orientation with respect to the crystallographic axes (for the case of wet etching at least). We suggest that the PL intensity quenching observed is due to exciton dissociation generated by some stray electric field, mainly oriented in the plane of the QWs, resulting from ion implantation in the regions close to the etched sidewalls. Previous studies have shown this kind of near-surface implantation to occur during RIE of Si surfaces by halogen-based gases. The details of this interaction still need to be investigated and revealed in details. This will

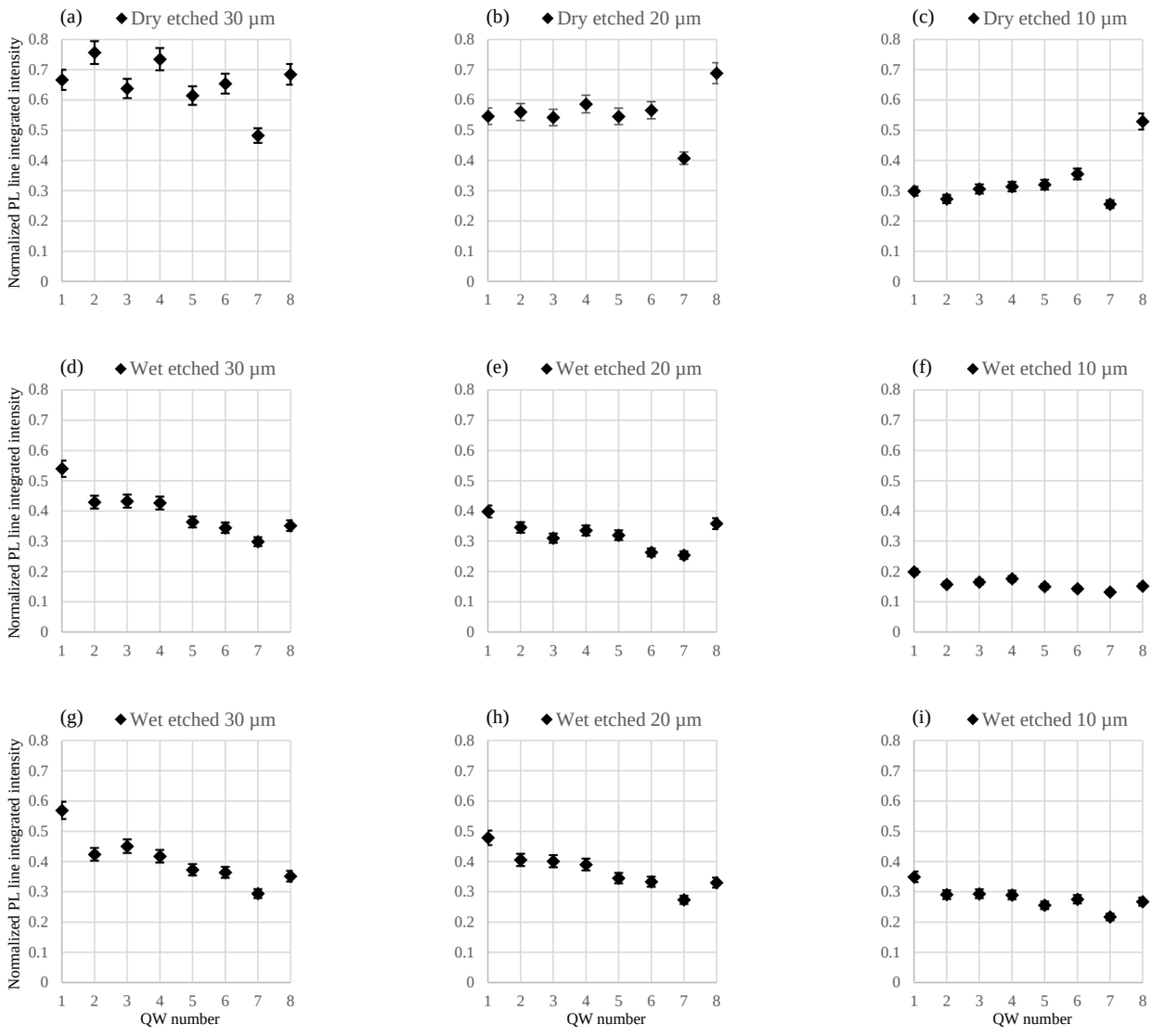

FIG. 9. PL intensities measured for the stripes etched with the different processes, as a function of the QW number, after normalization to the corresponding QW PL intensity measured on the reference sample (i.e. the epitaxial sample prior to any etching). (a-c) dry etched stripes, $< 0 \quad \bar{1} \quad 1 >$ orientation, 30, 20 and 10 μm; (d-f) wet etched stripes, $< 0 \quad \bar{1} \quad 1 >$ orientation, 30, 20 and 10 μm; (g-i) wet etched stripes, $< 0 \quad \bar{1} \quad \bar{1} >$ orientation, 30, 20 and 10 μm. Each point corresponds to the maximum intensity measured on the profiles shown in figs. 5 - 7.

be the purpose of a next phase of our study, as will be the proposal for a model for the development of the stray electric field and its interaction with the PL mechanisms.

ACKNOWLEDGMENTS

JPL and CL acknowledge support from the NanoRennes platform, affiliated to RENATECH+, the French national facilities network for micro-nanotechnology. RRL and ED acknowledge support from the Natural Sciences and Engineering Research Council of Canada (NSERC), Grant RGPIN-2018-04015. We also thank Julie Le Pouliquen for help with the etching and scanning electron microscopy observations.

REFERENCES

[1] A. Berrier, Y. Shi, J. Siegert, S. Marcinkevicius, S. He, and S. Anand, "Accumulated sidewall damage in dry etched photonic crystals," Journal of Vacuum Science and Technology B: Microelectronics and Nanometer Structures **27**, 1969 (2009).
[2] E. L. Hu and C.-H. Chen, "Dry Etch Damage in III-V Semiconductors," Microelectronic Engineering **35**, 23–28 (1997).
[3] M. de Lafontaine, E. Pargon, C. Petit-Etienne, G. Gay, A. Jaouad, M.-J. Gour, M. Volatier, S. Fafard, V. Aimez, and M. Darnon, "Influence of

plasma process on III-V/Ge multijunction solar cell via etching," Solar Energy Materials and Solar Cells **195**, 49–54 (2019).
[4]G. Morello, M. Quaglio, G. Meneghini, C. Papuzza, and C. Kompocholis, "Reactive ion etching induced damage evaluation for optoelectronic device fabrication," Journal of Vacuum Science & Technology B: Microelectronics and Nanometer Structures **24**, 756 (2006).
[5]N. P. Siwak, X. Z. Fan, and R. Ghodssi, "Fabrication challenges for indium phosphide microsystems," Journal of Micromechanics and Microengineering **25**, 043001 (2015).
[6]S. J. Pearton, F. Ren, C. R. Abernathy, W. S. Hobson, T. R. Fullowan, R. Esagui, and J. R. Lothian, "Damage introduction in InP and InGaAs during Ar and H_2 plasma exposure," Applied Physics Letters **61**, 586–588 (1992).
[7]S. Pearton, "Critical issues of III–V compound semiconductor processing," Materials Science and Engineering: B **44**, 1–7 (1997).
[8]J. J. Kelly and H. G. Philipsen, "Anisotropy in the wet-etching of semiconductors," Current Opinion in Solid State and Materials Science **9**, 84–90 (2005).
[9]S. J. Pearton, "Reactive ion etching of III–V semiconductors," International Journal of Modern Physics B , 1781–1876 (1994).
[10]V. M. Donnelly and A. Kornblit, "Plasma etching: Yesterday, today, and tomorrow," Journal of Vacuum Science & Technology A: Vacuum, Surfaces, and Films **31**, 050825 (2013).
[11]J. P. Landesman, N. Isik-Goktas, R. R. LaPierre, C. Levallois, S. Ghanad-Tavakoli, E. Pargon, C. Petit-Etienne, and J. Jiménez, "Low temperature micro-photoluminescence spectroscopy of microstructures with InAsP/InP strained quantum wells," Journal of Physics D: Applied Physics **54**, 445106 (2021).
[12]J.-P. Landesman, J. Jiménez, C. Levallois, F. Pommereau, C. Frigeri, A. Torres, Y. Léger, A. Beck, and A. Rhallabi, "Defect formation during chlorine-based dry etching and their effects on the electronic and structural properties of InP/InAsP quantum wells," Journal of Vacuum Science & Technology A: Vacuum, Surfaces, and Films **34**, 041304 (2016).
[13]P. H. L. Notten, "The Etching of InP in HCl Solutions: A Chemical Mechanism," Journal of The Electrochemical Society **131**, 2641–2644 (1984).
[14]C. M. Haapamaki, *Growth of InAs/InP Nanowires by Molecular Beam Epitaxy*, Ph.D. thesis, McMaster University, Hamilton, ON Canada p. 20-26 (2012).
[15]C. Monier, M. F. Vilela, I. Serdiukova, and A. Freundlich, "Photocurrent and photoluminescence spectroscopy of $InAs_xP_{1-x}$/InP strained quantum wells grown by chemical beam epitaxy," Journal of Crystal Growth **188**, 332–337 (1998).
[16]H. Q. Hou and C. W. Tu, "Optical property of InAsP/InP strained quantum wells grown on InP (111) *B* and (100) substrates," Journal of Applied Physics **75**, 4673–4679 (1994).
[17]Nextnano, www.nextnano.de.
[18]Y.-G. Zhao, R. A. Masut, J. L. Brebner, C. A. Tran, and J. T. Graham, "Temperature dependence of photoluminescence in InAsP/InP strained multiple quantum wells," Journal of Applied Physics **76**, 5921–5926 (1994).
[19]S. Finot, C. Le Maoult, E. Gheeraert, D. Vaufrey, and G. Jacopin, "Surface Recombinations in III-Nitride Micro-LEDs Probed by Photon-Correlation Cathodoluminescence," ACS Photonics **9**, 173–178 (2022).
[20]W. Van Roosbroeck, "Injected Current Carrier Transport in a Semi-Infinite Semiconductor and the Determination of Lifetimes and Surface Recombination Velocities," Journal of Applied Physics **26**, 380–391 (1955).
[21]C. Becht, U. T. Schwarz, M. Binder, and B. Galler, "Diffusion Analysis of Charge Carriers in InGaN/GaN Heterostructures by Microphotoluminescence," physica status solidi (b) **260**, 2200565 (2023).
[22]A. Fiore, M. Rossetti, B. Alloing, C. Paranthoen, J. X. Chen, L. Geelhaar, and H. Riechert, "Carrier diffusion in low-dimensional semiconductors: A comparison of quantum wells, disordered quantum wells, and quantum dots," Physical Review B **70**, 205311 (2004).
[23]V. Malyarchuk, J. W. Tomm, V. Talalaev, C. Lienau, F. Rinner, and M. Baeumler, "Nanoscopic measurements of surface recombination velocity and diffusion length in a semiconductor quantum well," Applied Physics Letters **81**, 346–348 (2002).
[24]A. Bensaada, R. Cochrane, R. Masut, R. Leonelli, and G. Kajrys, "Surface morphology and lattice distortion of heteroepitaxial GaInP on InP," Journal of Crystal Growth **130**, 433–443 (1993).
[25]H. F. Winters, D. B. Graves, D. Humbird, and S. Tougaard, "Penetration of fluorine into the silicon lattice during exposure to F atoms, F2, and XeF2: Implications for spontaneous etching reactions," Journal of Vacuum Science & Technology A: Vacuum, Surfaces, and Films **25**, 96–103 (2007).
[26]D. A. B. Miller, D. S. Chemla, T. C. Damen, A. C. Gossard, W. Wiegmann, T. H. Wood, and C. A. Burrus, "Electric field dependence of optical absorption near the band gap of quantum-well structures," Physical Review B **32**, 1043–1060 (1985).

DATA AVAILABILITY

The data that support the findings of this study are available from the corresponding author upon reasonable request.